

Spin Torque, Tunnel-Current Spin Polarization, and Magnetoresistance in MgO Magnetic Tunnel Junctions

G. D. Fuchs,¹ J. A. Katine,² S. I. Kiselev,² D. Mauri,² K. S. Wooley,¹ D. C. Ralph,¹ and R. A. Buhrman¹

¹Cornell University, Ithaca, New York 14853-2501, USA

²Hitachi Global Storage Technologies, San Jose, California 95120, USA

(Received 28 October 2005; published 9 May 2006)

We employ the spin-torque response of magnetic tunnel junctions with ultrathin MgO tunnel barrier layers to investigate the relationship between spin transfer and tunnel magnetoresistance (TMR) under finite bias, and find that the spin torque per unit current exerted on the free layer decreases by $<10\%$ over a bias range where the TMR decreases by $>40\%$. This is inconsistent with free-electron-like spin-polarized tunneling and reduced-surface-magnetism models of the TMR bias dependence, but is consistent with magnetic-state-dependent decay lengths in the tunnel barrier.

DOI: 10.1103/PhysRevLett.96.186603

PACS numbers: 72.25.-b, 75.75.+a, 85.75.-d

The ability of electron currents to transfer spin, as well as charge, from one ferromagnetic electrode to another, and hence to exert spin torque on the electrodes (see, e.g., Refs. [1,2]), provides a powerful new tool for the study of spin transport in electronic structures, in addition to establishing new opportunities for future applications [2,3]. The related issue of spin-dependent electron transport in magnetic multilayer structures, both magnetic tunnel junctions (MTJs) [4] and spin valves [5], is of widespread interest, both fundamentally and because of the importance this phenomenon has for information storage [6,7]. A critical aspect of MTJs is the bias dependence of the tunnel magnetoresistance (TMR) (see, e.g., Ref. [8]) which, in general, decreases as the voltage bias (V) increases. Currently, there is no consensus as to a microscopic model that accounts for this behavior. Here we report our study of the relationship between bias dependent TMR and spin torque, which is fundamental to understanding both the nature of spin-polarized tunneling at finite bias and spin-transfer effects in MTJs [9–11]. By making measurements of the thermally activated switching of nanostructured MTJs, we determine the bias dependence of the spin torque transferred across an MgO tunnel barrier and its relation to the TMR. The spin torque per unit current is, within 10%, a constant function of V up to ± 0.35 V in our devices, in contrast to the TMR, which is reduced by $>40\%$ at ± 0.35 V. This behavior is inconsistent with a decrease in the polarization factors of the electrodes as described by free-electron tunneling models [12–14] or by surface-magnon emission models that substantially decrease the surface magnetization with increasing bias [15]. We find, however, that magnetic-state-dependent tunneling decay lengths (effective masses) as theoretically predicted to result in very high TMR in MgO tunnel barriers [16–18] are consistent with our results, if we include the effects of our ultrathin-barrier layers having a high density of atomic defects and lower barrier heights than ideal MgO barriers.

We fabricated our MTJs by sputtering multilayer films on an unpatterned substrate that consisted of (in nm) the

following: Ta 3/Cu 28.5/Ta 3/PtMn 15.4/CoFe 1.9/Ru 0.7/CoFe 2.2/MgO 0.8/CoFe 1.0/Py 1.8/Ru 1.5/Ta 3.0/Cu 10, where CoFe is $\text{Co}_{90}\text{Fe}_{10}$ and Py is $\text{Ni}_{91.5}\text{Fe}_{8.5}$. The devices were formed into a nanopillar geometry using procedures described elsewhere [19]. The “free layer” for these devices is the CoFe/Py bilayer, and the “reference layer” is an exchange coupled [20] CoFe/Ru/CoFe structure, strongly pinned by the antiferromagnet PtMn layer, that exerts a small (~ 0 –140 Oe) dipolar field H_{dip} on the free layer due to magnetostatic edge charges.

Figure 1(a) shows the dc resistance TMR response of sample 1, which has a free layer in the form of a 50×100 nm elongated hexagon with an area of 3.5×10^{-11} cm^2 , as H is swept through H_{dip} . The small magnetic volume of the free layer in this sample causes it to be thermally unstable at room temperature (RT), so when $(H - H_{\text{dip}}) \sim 0$ there is almost no torque due to H , and the nanomagnet telegraphs between two stable states, nominally parallel (P, low resistance) and antiparallel (AP, high resistance) with respect to the reference layer. Throughout, we define $\text{TMR} = \Delta R/R_p$. Because of the low specific resistance of these junctions ($\sim 5 \Omega \mu\text{m}^2$), the tunnel current at accessible bias is large enough to exert a spin-transfer torque N_{st} on the free layer that is comparable in magnitude to the field torque N_H . N_H and N_{st} are not collinear, but nevertheless we can apply H and I so that N_H

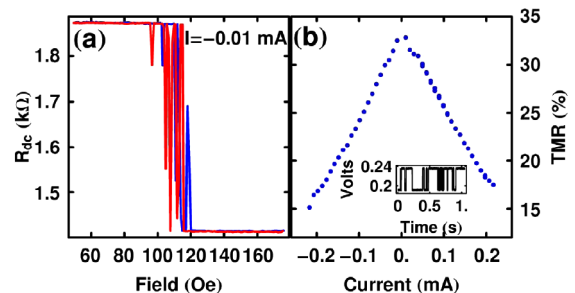


FIG. 1 (color online). (a) R_{dc} vs H for sample 1. (b) TMR vs I for sample 1 calculated from telegraph traces (inset).

and N_{st} have equal but opposing effects on the energy barrier for magnetic reversal. This condition is met whenever the mean lifetimes ($\tau_{P/AP}$) of the two stable resistance states are equal as determined from time traces of the telegraph behavior [Fig. 1(b), inset] at a given H and I . By varying H we can examine the spin torque at bias levels ranging from very low I up to the point where the tunnel barrier begins to degrade due to the high I . In this range the TMR decreases from 33% (zero bias) to 19% (0.35 V bias).

The $H(I)$ for equal lifetimes of sample 1 at RT is plotted in Fig. 2(a). The data follow a straight line for negative currents and positive currents up to $I \sim 0.1$ mA (region 1), after which there is a change in the behavior of the sample to a second linear region (region 2). In Fig. 2(b) we show results for another device, sample 2, which also exhibits two regions of linear behavior with the break occurring in this device at $I \sim -0.03$ mA. Notice that here the break results in a higher linear slope for positive I , opposite to the case for sample 1. We made similar RT telegraph switching measurements on six other MTJ samples, and they all have similar behavior, typically exhibiting one break in the linear equal-lifetime behavior, with this break occurring at either positive or negative I . Furthermore, the $H(I)$ data for a given sample is highly reproducible.

Since the behavior of the equal-lifetime data is central to this study, we investigated the origin of the breaks in the data by cooling sample 1 to 5.6 K and found two distinct sets of nominally P and AP states that were randomly occupied when H was ramped to cycle the free layer hysteretically between P and AP alignment. These two sets of states had different coercive fields, as well as slightly different (<2% difference) resistance values for nominal P and AP alignment. This indicated that, due to microcrystalline anisotropy effects [20], the sample had two slightly different micromagnetic states that were sepa-

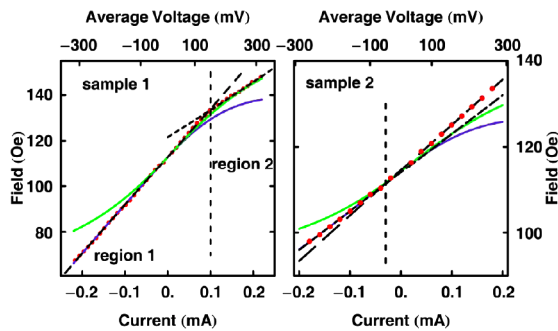


FIG. 2 (color online). Plot of values of $H(I)$ for equal lifetimes of two level resistance fluctuations in samples 1 and 2. The top axis indicates the average of the voltage of the two states [slightly nonlinear scale due to $I(V)$ characteristics]. The diagonal dashed lines are fits with $\gamma(I) = 1$ for region 1 and region 2. The solid purple or dark gray (green or light gray) lines are the calculated position of equal lifetime assuming $\gamma(I)$ is described by the free-electron split-band model (reduced surface magnetization model). The vertical dashed lines separate the two regions of linear behavior for each sample.

rated by a small energy barrier, and therefore were directly distinguishable only in TMR scans at low temperature.

As discussed later, when we fit the RT equal-lifetime data to the standard spin-torque model we found that the two coercive fields of sample 1 measured at 5.6 K were closely consistent with the two different RT coercive fields that were obtained from the best fits to the two linear regions of the $H(I)$ data. This indicates that the spin-torque bias determines which micromagnetic state is preferred at RT. Finally, to verify that the breaks in $H(I)$ are not due to intrinsic tunneling behavior, we also made measurements of spin valve nanopillars with the same size and layer structure, with 2 nm of Cu replacing the MgO, and found that they also had breaks in their linear $H(I)$ behavior.

The mean lifetime of a Néel-Brown magnetic particle in a given state ($\tau_{P/AP}$) as a function of H and I is [21–24]

$$\tau_{P/AP} = \tau_o \exp \left[\frac{E_a}{k_B T} \left(1 \pm \frac{H - H_{dip}}{H_{c,o}} \right)^\alpha \left(1 \mp \frac{I\gamma(I)}{I_{c,o}^{P/AP}} \right) \right], \quad (1)$$

where $\tau_o = 10^{-9}$ s is the attempt time, E_a is the thermal activation barrier, T is the temperature, $H_{c,o}$ is the $T = 0$ coercive field, $I_{c,o}^{P/AP}$ is the $T = 0$ K critical current for switching from the P state (/AP state), α is either 2 or 3/2 [25], and $\gamma(I)$ parametrizes how N_{st}/I varies with I (or with V). In addition, we normalize $\gamma(0) = 1$. This formula is valid in the thermal activation regime where $H_{c,o}$ is substantially larger than $(H - H_{dip})$ and where $I_{c,o}$ is somewhat larger than I . The condition $\tau_P = \tau_{AP}$ allows us to calculate the predicted $H(I)$ for equal lifetimes, with the result being a linear relationship with a slope that depends on $I_{c,o}^P$, $I_{c,o}^{AP}$, $H_{c,o}$, and α , provided $\gamma(I) = \text{const}$. Figure 2 demonstrates that, apart from the breakpoints, the $H(I)$ data exhibit straight lines, indicating that the spin-torque efficiency is essentially constant over the bias range.

Figure 3(a) shows the equal lifetime plotted vs I . Away from the micromagnetic breakpoints, the lifetime data can be utilized to obtain values for the device spin-torque parameters by fitting the data to Eq. (1). It is necessary to account for the significant self-heating in the MTJs, which varies as [26] $T = \sqrt{T_{bath}^2 + \beta I^2}$, where T_{bath} is the bath temperature and β parametrizes the heating and is proportional to the resistance and geometry specific factors. For region 1 of sample 1, if we set $\gamma(I) = 1$ and assume $\alpha = 2$, we find that $\beta = (8.5 \pm 0.3) \times 10^5$ K/mA², which is consistent with that found in previous MTJ spin-transfer studies, and $E_{a,1} = 0.51 \pm 0.01$ eV. This activation energy is comparable to, but somewhat less than, the nominal value of ~ 0.74 eV for ideal single domain rotation calculated by $E_a = H_{c,o} M_s \text{Vol}/2$, where M_s is the saturation magnetization and Vol is the volume of the free layer. We also find that for region 1, $I_{c,o}^P = 0.97 \pm 0.02$ mA, $I_{c,o}^{AP} = 0.77 \pm 0.01$ mA, and $H_{c,o}$ (region 1) = 350 ± 10 Oe. This latter value is in very good agreement with the value $H_{c,o} = 348 \pm 10$ Oe obtained by correcting the higher of the two measured

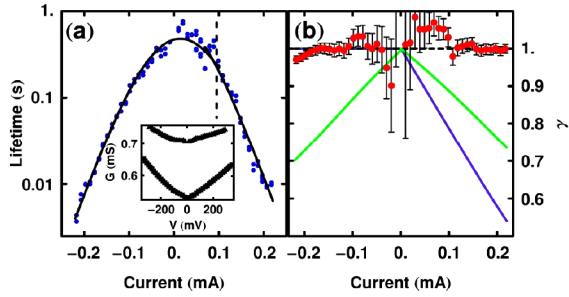


FIG. 3 (color online). (a) Lifetimes of sample 1 plotted against I . Solid lines are fits in each of the two regions of magnetic behavior. The inset shows the conductance ($G = I/V$) of each state, calculated from the time traces, as a function of V . (b) $\gamma(I)$ data calculated as described in the text. The solid lines represent the prediction of $\gamma(I)$ calculated using the free-electron split-band model (purple or dark gray) and the reduced surface magnetization model (green or light gray) from the TMR(I) data.

$T = 5.6$ K coercive fields for sample 1 for the change in saturation magnetization (M_s) between 5.6 K and RT [27]. Assuming that the critical currents and β are essentially the same in region 2 as in region 1, we obtain $E_{a,2} = 0.53 \pm 0.01$ eV and $H_{c,o}$ (region 2) = 285 ± 10 Oe, where the latter is also in excellent agreement with the value $H_{c,o} = 282 \pm 10$ Oe obtained from the other coercive field found at low T for this sample.

To further test our conclusion that $\gamma(I) \sim 1$ and $N_{st}/I \sim \text{const}$ within experimental error (for -0.35 V $< V < 0.35$ V), we extracted $\gamma(I)$ explicitly from the data [Fig. 3(b)]. This was done by using the parameters determined above to calculate $\gamma(I)$ from differences between the $H(I)$ data and the $H(I)$ fit. At small I , the uncertainty is larger since both I and $(H - H_{\text{dip}})$ are small, and uncertainties in the determination of H at equal lifetimes are more important. We also performed fits of the data in which we allowed $\gamma(I)$ to vary linearly. In both cases, we can set a limit that $\gamma(I)$ decreases by less than 10%.

The constancy of $\gamma(I)$ over the accessible bias range (0–0.35 V) has implications for various models used to interpret the decrease in TMR(V) observed in MTJs. In split-band free-electron models [12,13] the decrease in TMR with increasing V is due to changes in the effective polarization (P_{col}) of the collector electrode at energy eV above the Fermi level. The effective polarization of the emitter (P_{emit}) in these models remains constant, as the electrons tunnel from the same set of states near the Fermi energy. Since the TMR, given by Julliere's formula [4], $\text{TMR} = \Delta R/R_p = 2P_{\text{col}}P_{\text{emit}}/(1 - P_{\text{col}}P_{\text{emit}})$, is sensitive to the product of the polarization factors, it decreases for both directions of I . In contrast, in these models the magnitude of N_{st}/I [and hence $\gamma(I)$] on a given layer is proportional only to the effective polarization of the counter electrode [11]. Since we designed our devices so that only the free layer is responsive to spin torque, there is an asymmetry imposed by V . For negative I , the reference layer is the emitter, whose polarization factor remains constant. For

positive I , however, the reference layer is the collector, which according to the free-electron model has a decreasing polarization factor with increasing V . Using Julliere's formula, the free-electron model's prediction for $\gamma(I)$ can be calculated from the TMR data [28]:

$$\gamma(I) = \frac{\text{TMR}(I)}{2 + \text{TMR}(I)} \left(\frac{2 + \text{TMR}_{\text{max}}}{\text{TMR}_{\text{max}}} \right) \quad \text{for } I > 0; \quad (2)$$

$$\gamma(I) = 1 \quad \text{for } I < 0.$$

This predicted form of $\gamma(I)$, calculated from our TMR data, is plotted in Fig. 3(b), while Fig. 2 shows the prediction for the $H(I)$ equal-lifetime data. The prediction that $\gamma(I)$ should be reduced to ~ 0.6 at $I \sim 0.2$ mA is clearly inconsistent with our measurements.

A second proposed mechanism for TMR(V) is hot electron emission of surface magnons that reduces the surface magnetization through the population of surface-magnon modes [15]. If this is a symmetrical process, it will decrease the polarization factors of the electrodes by an equal amount, and therefore

$$\gamma(I) = \sqrt{\frac{\text{TMR}(I)}{2 + \text{TMR}(I)} \left(\frac{2 + \text{TMR}_{\text{max}}}{\text{TMR}_{\text{max}}} \right)}, \quad (3)$$

which, at the highest bias studied, would cause $\gamma(I)$ to decrease to ~ 0.7 [Fig. 3(b)]. The effect of this form of $\gamma(I)$ on the $H(I)$ data for both samples is plotted in Fig. 2, which shows a substantial deviation from the measurement result. We note that while for sample 1, the slope change at positive I causes an approximate overlap of the data with the predicted $H(I)$ behavior for that bias polarity, there is a strong deviation for both current directions for sample 2.

Two other mechanisms that have been invoked to explain TMR(V) have unclear consequences for the spin torque of MTJs. These are electron spin flip via magnon emission during tunneling [29,30] and impurity assisted resonant tunneling [31]. In light of our spin-torque results we can conclude that if either of these processes plays a role in the tunnel conductance of our MTJ devices, they do not act to decrease N_{st}/I .

The behavior of our devices can, however, be understood within the framework of the same theory [16–18] that predicts the very large TMR achieved with epitaxial Fe/MgO/Fe MTJ and related systems [32,33]. This large TMR is attributed to symmetry considerations in the overlap of the spin-dependent electronic wave functions between the Fe electrodes and MgO tunnel barriers. In bcc Fe, majority electrons have either s -like or pd -like character. When the electrodes are aligned in the P state, the s -like electrons tunnel through the MgO with a smaller effective mass m^* , i.e., a longer tunnel decay length, than those with pd -like character. As a result, it is the s -like electrons that dominate the majority-to-majority tunneling processes in thick, well-formed barrier layers. The minority electrons, having pd -like character, have a much lower tunneling rate, yielding a high tunnel polarization. When

the electrodes are aligned in AP configuration, in the assumed case of coherent tunneling, i.e., in the absence of scattering, only the majority (minority) electrons with pd -like character can tunnel into minority (majority) states of the collector with the same symmetry. Because of the band structure of MgO, m^* for these electrons is higher and hence the tunnel decay length is shorter. This gives rise to two related effects; the predicted TMR at low bias is very high due to the reduced conductance in the AP configuration, and the different m^* 's result in the AP conductance increasing more rapidly with V at high bias than the P conductance, which results in a decreasing TMR(V) without a decrease in the polarization of the tunnel current for a given magnetic configuration (AP or P).

Unlike thicker MgO tunnel barrier devices that experimentally show very high TMR, the ultrathin-barrier MgO MTJ's studied here have far from ideal TMR behavior with $\sim 30\%$ TMR at low bias, indicating the coherent tunneling process has been diluted. Recent scanning tunneling spectroscopy studies have found that textured (001) ultrathin MgO layers grown by sputtering or e -beam evaporation on Fe and CoFe(001) surfaces have a substantial density of oxygen vacancies, with a higher density in the thinner layers, presumably due to an unrelaxed lattice mismatch [34]. The presence of such defect states introduces the possibility of momentum scattering processes such as co-tunneling, which allow some pd -like electrons to scatter elastically and tunnel as s -like states and vice versa, reducing the TMR. In addition, since our bias range (± 0.35 V) is a significant fraction of the tunnel barrier height (~ 0.5 eV), the high m^* electrons, both majority and minority, that dominate in the AP configuration only have a strong voltage-dependent conductance increase, causing a strong bias dependence of the TMR. Since such momentum scattering is spin independent, these effects enhance the tunnel conductance without affecting the spin current, which leads to an approximately constant N_{st}/I for each magnetic configuration that is consistent with our experimental result. Fitting the $I(V)$ characteristic of each magnetic state with the Simmons model [35] yields a significantly larger m^* for the AP configuration, and is consistent with this picture of the conduction.

In conclusion, we have studied the bias dependence of the spin-torque response of a MTJ with an ultrathin MgO tunnel barrier and a thermally unstable free layer at room temperature. The spin torque transferred between the reference layer and the free layer per unit current decreases less than 10% up to $\sim \pm 0.35$ V, at which point the TMR level has decreased by over 40%. This observation sheds new light on the process of TMR reduction with bias by imposing additional constraints on any model that describes this process. We find that the data can be well described by a magnetic-orientation-dependent difference between the effective masses for tunneling, which causes the conductance to increase more rapidly in the AP state than in the P state, while preserving the polarization of the

tunnel current in each state, and hence the efficiency of the spin-transfer torque at increasing bias.

We thank P. Brouwer and S. Adam for very useful conversations, and P. Mather for sharing STS data. This work is supported by ARO/MURI (DAA19-01-0-0541) and NSF through the NSEC support of the Center for Nanoscale Systems. Additional support is provided by NSF through use of the NNIN/CNF facilities and the facilities of the Cornell MRSEC.

-
- [1] J. A. Katine *et al.*, Phys. Rev. Lett. **84**, 3149 (2000).
 - [2] S. I. Kiselev *et al.*, Nature (London) **425**, 380 (2003).
 - [3] F. J. Albert *et al.*, Appl. Phys. Lett. **77**, 3809 (2000).
 - [4] M. Julliere, Phys. Lett. **54A**, 225 (1975).
 - [5] M. N. Baibich *et al.*, Phys. Rev. Lett. **61**, 2472 (1988).
 - [6] S. Tehrani *et al.*, Proc. IEEE **91**, 703 (2003).
 - [7] S. S. P. Parkin *et al.*, Proc. IEEE **91**, 661 (2003).
 - [8] J. S. Moodera and G. Mathon, J. Magn. Magn. Mater. **200**, 248 (1999).
 - [9] Y. Huai *et al.*, Appl. Phys. Lett. **84**, 3118 (2004).
 - [10] G. D. Fuchs *et al.*, Appl. Phys. Lett. **85**, 1205 (2004).
 - [11] J. C. Slonczewski, Phys. Rev. B **71**, 024411 (2005).
 - [12] J. C. Slonczewski, Phys. Rev. B **39**, 6995 (1989).
 - [13] X. Zhang *et al.*, Phys. Rev. B **56**, 5484 (1997).
 - [14] S. O. Valenzuela *et al.*, Phys. Rev. Lett. **94**, 196601 (2005).
 - [15] J. S. Moodera *et al.*, Phys. Rev. Lett. **80**, 2941 (1998).
 - [16] W. H. Butler *et al.*, Phys. Rev. B **63**, 054416 (2001).
 - [17] J. Mathon and A. Umerski, Phys. Rev. B **63**, 220403(R) (2001).
 - [18] X.-G. Zhang and W. H. Butler, Phys. Rev. B **70**, 172407 (2004).
 - [19] D. Lacour *et al.*, Appl. Phys. Lett. **85**, 4681 (2004).
 - [20] The existence of microcrystalline anisotropy in the free layer material was confirmed by magnetoresistance measurements on circular spin valves with the same free layer, which yielded microcrystalline anisotropy fields that, while reproducible, varied from 110 to 240 Oe along random directions in the eight samples studied.
 - [21] E. B. Myers *et al.*, Phys. Rev. Lett. **89**, 196801 (2002).
 - [22] R. H. Koch, J. A. Katine, and J. Z. Sun, Phys. Rev. Lett. **92**, 088302 (2004).
 - [23] Z. Li and S. Zhang, Phys. Rev. B **68**, 024404 (2003).
 - [24] I. N. Krivorotov *et al.*, Phys. Rev. Lett. **93**, 166603 (2004).
 - [25] R. H. Victora, Phys. Rev. Lett. **63**, 457 (1989).
 - [26] G. D. Fuchs *et al.*, Appl. Phys. Lett. **86**, 152509 (2005).
 - [27] S. Maat *et al.*, Phys. Rev. B **70**, 014434 (2004).
 - [28] Since we have conducted our experiment in constant current mode, the calculation of TMR(I) is more appropriate than TMR(V). This results in a 2% larger TMR decrease, which is insignificant to our analysis.
 - [29] S. Zhang *et al.*, Phys. Rev. Lett. **79**, 3744 (1997).
 - [30] M. Elsen *et al.*, Phys. Rev. B **73**, 035303 (2006).
 - [31] E. Y. Tsybal *et al.*, Phys. Rev. Lett. **90**, 186602 (2003).
 - [32] S. S. P. Parkin *et al.*, Nat. Mater. **3**, 862 (2004).
 - [33] S. Yuasa *et al.*, Nat. Mater. **3**, 868 (2004).
 - [34] P. G. Mather, J. C. Read, and R. A. Buhrman, cond-mat/0603734.
 - [35] J. G. Simmons, J. Appl. Phys. **34**, 1793 (1963).